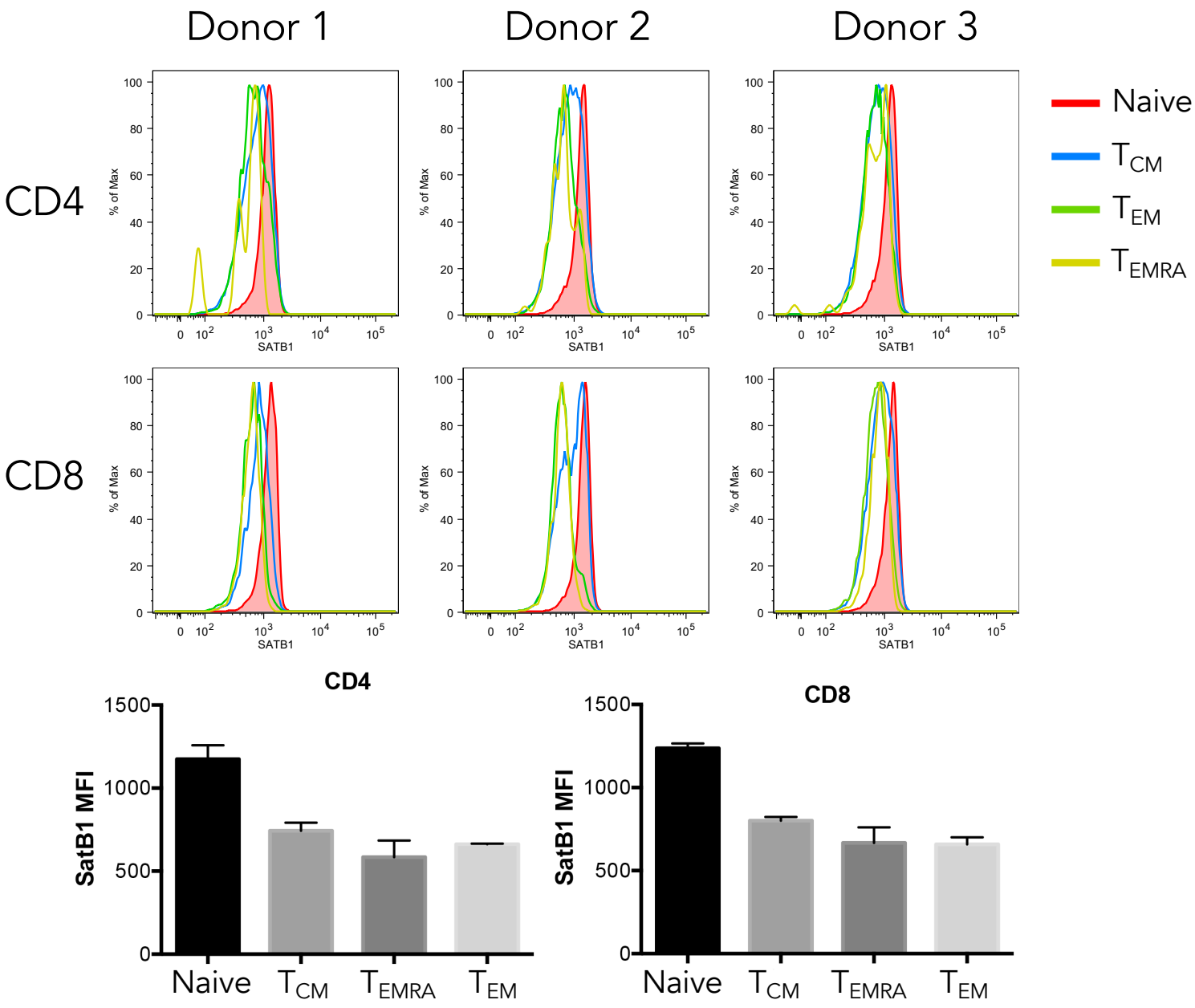

Supplementary figure 1. SATB1 expression in human CD8$^+$ T cell subsets. Human peripheral blood mononuclear cells were immuno-stained for flow cytometry to measure proportions naïve (CD27$^+$CD45RA$^+$), T_{CM} (CD27$^+$CD45RA$^-$), TEMRA (CD27$^-$CD45RA$^+$) and TEM (CD27$^-$CD45RA$^-$) CD4$^+$ and CD8$^+$ T cells. Shown are representative histograms and SATB1 mean fluorescence intensity.

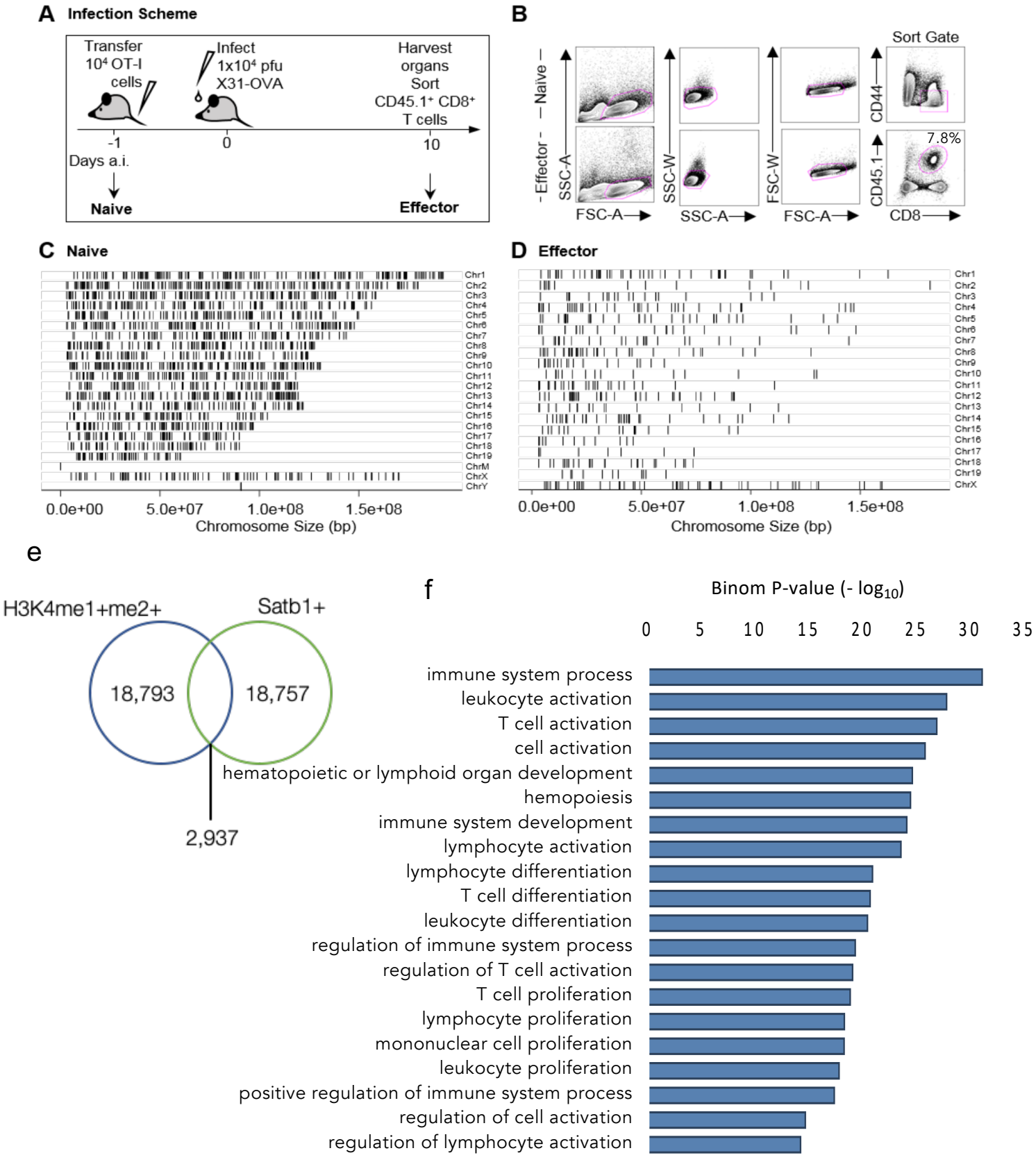

Supplementary figure 2. SATB1 binding profiles within naïve and effector CD8+ T cells. **(a)** SATB1 ChIP-seq was performed on either naïve ($CD44^{lo}CD62L^{hi}$) OTIs or effector OT-I isolated from recipient mice after adoptive transfer and subsequent infection with x31-OVA. **(b)** Representative sort profiles of naïve $CD44^{lo}CD8^{+}$ OT-I T cells from spleens of uninfected mice or effector OT-I $CD8^{+}$ T cells. **(c, d)** SATB1 binding sites identified mapped onto individual chromosomes in naïve **(c)** or **(d)** effector OT-I CD8+ T cells using the Chipseeker R-package. **(e)** SATB1 binding sites within naïve CD8+ OTIs was overlaid with naïve OT-I $CD8^{+}$ H3K4me1 and H3K4me2 ChIP seq data (Russ *et al*, 2017). Shown is the number of peaks that overlap. **(f)** Gene ontology analysis was performed on the nearest neighboring genes to SATB1 binding peaks observed in naïve $CD8^{+}$ OT-Is. Biological pathways are ranked according to -log10 p-values using the GREAT (3.0) software.

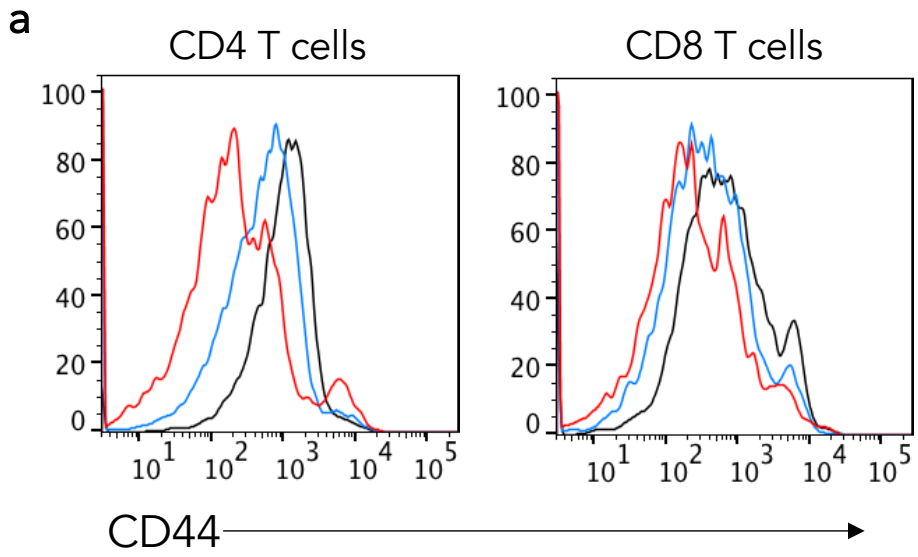

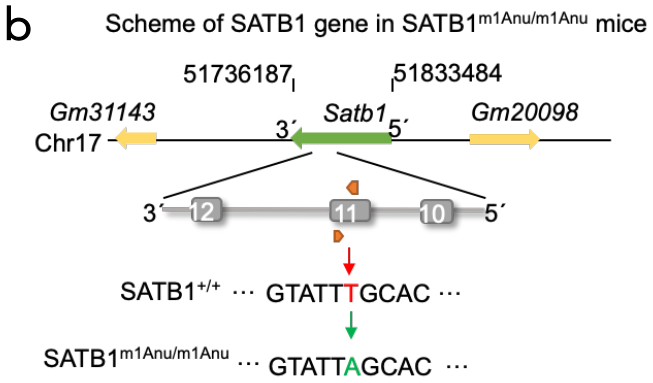

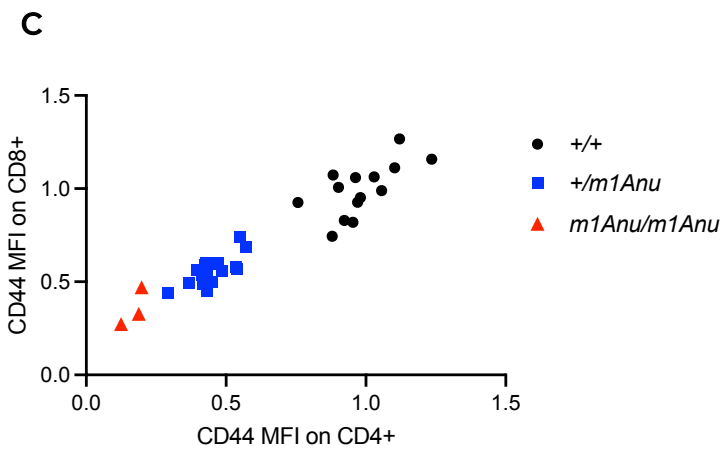

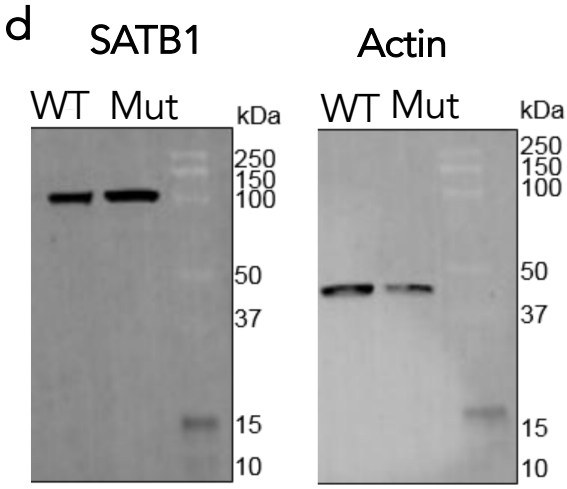

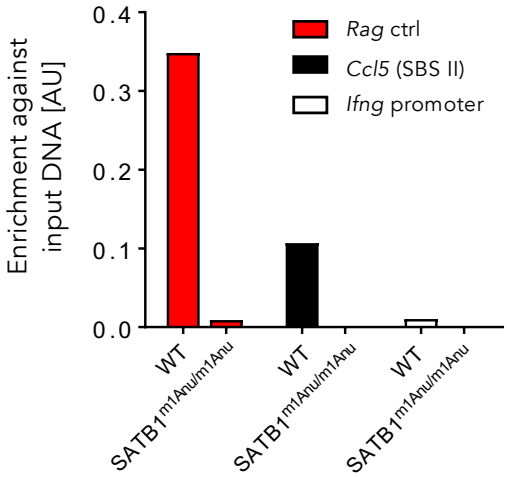

Supplementary figure 3. Identification and characterization of SATB1^{m1Anu} mice. **(a)** representative histograms showing CD44 expression on naïve CD4+ T cells. **(b)** Identification of the point mutation in exon 11 of the SATB1 gene (T->A mutation) after ENU mutagenesis. **(c)** Quantitation of CD44 expression on WT, heterozygous and homozygous mice. **(d)** Western blot of SATB1 and beta-ACTIN from same samples after loading 10 µg of protein from thymocytes from WT and SATB1$^{m1Anu/m1Anu}$ (Mut) mice. **(e)** SATB1 ChIP was performed on SATB1 binding sites predicted from the ChIP-seq data that included a region distal to *Rag* locus, a binding site upstream of *Ccl5* locus and a a negative control within the IFNγ promoter that showed no evidence of SATB1 binding.

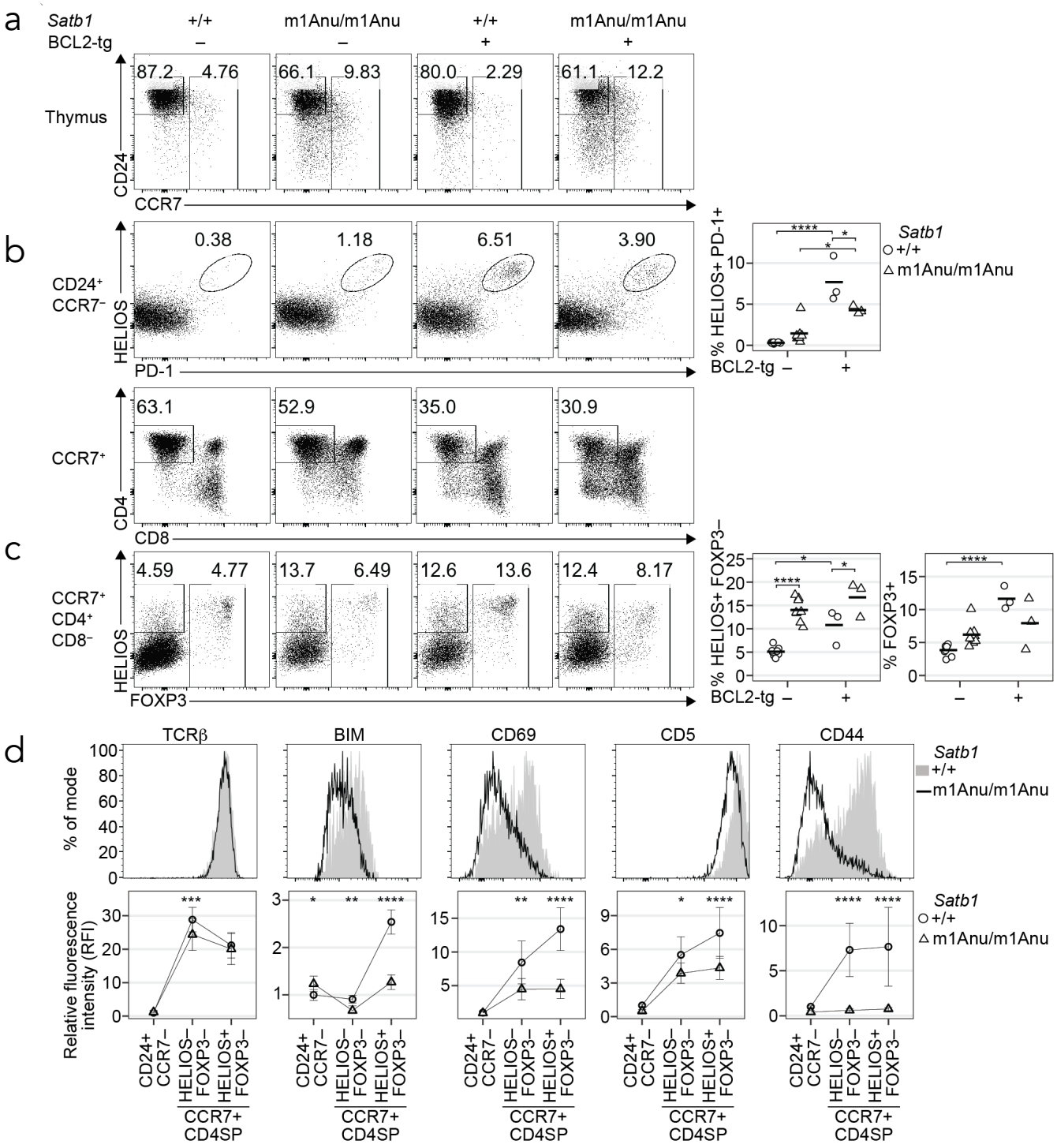

Supplementary figure 4. Perturbation of thymic selection within SATB1$^{m1Anu/m1Anu}$ thymocytes. **(a)** CD24/CCR7 and CD4/CD8 phenotype of thymocytes from mice with the indicated genotypes (top) with a gate for the CD24$^+$ CCR7 population. **(b)** Analysis of CD24$^+$/CCR7$^+$ thymocytes were analysed for Helios and PD-1 expression to enumerate the Helios+ PD-1+ subset (right). **(c)** CD4$^{+/}$CCR7$^+$ phenotype of CCR7+ thymocytes, with a gate for the CD4SP population, analysed for Helios and Foxp3 expression to enumerate the Helios+ Foxp3 and Foxp3+ subsets (right). **(d)** Histogram overlays show TCRβ, BIM, CD69, CD5 and CD44 within CD24$^+$/CCR7+ CD4SP HELIOS$^+$ subsets. Graphs (below) show relative fluorescence intensities (RFI) of TCRβ, BIM, CD69, CD5 and CD44 within CCR7$^+$CD4SP thymocytes subsets of in concatenated FACS files from a single experiment. Circles represent WT mice (SATB1$^{+/+}$) and triangles represent SATB1m1Anu/^{m1Anu} mice. Statistical analyses used 2-way ANOVA with Sidak's multiple comparisons test. *P*-values: * $P < 0.05$, ** $P < 0.01$, *** $P < 0.001$ and **** $P < 0.0001$.

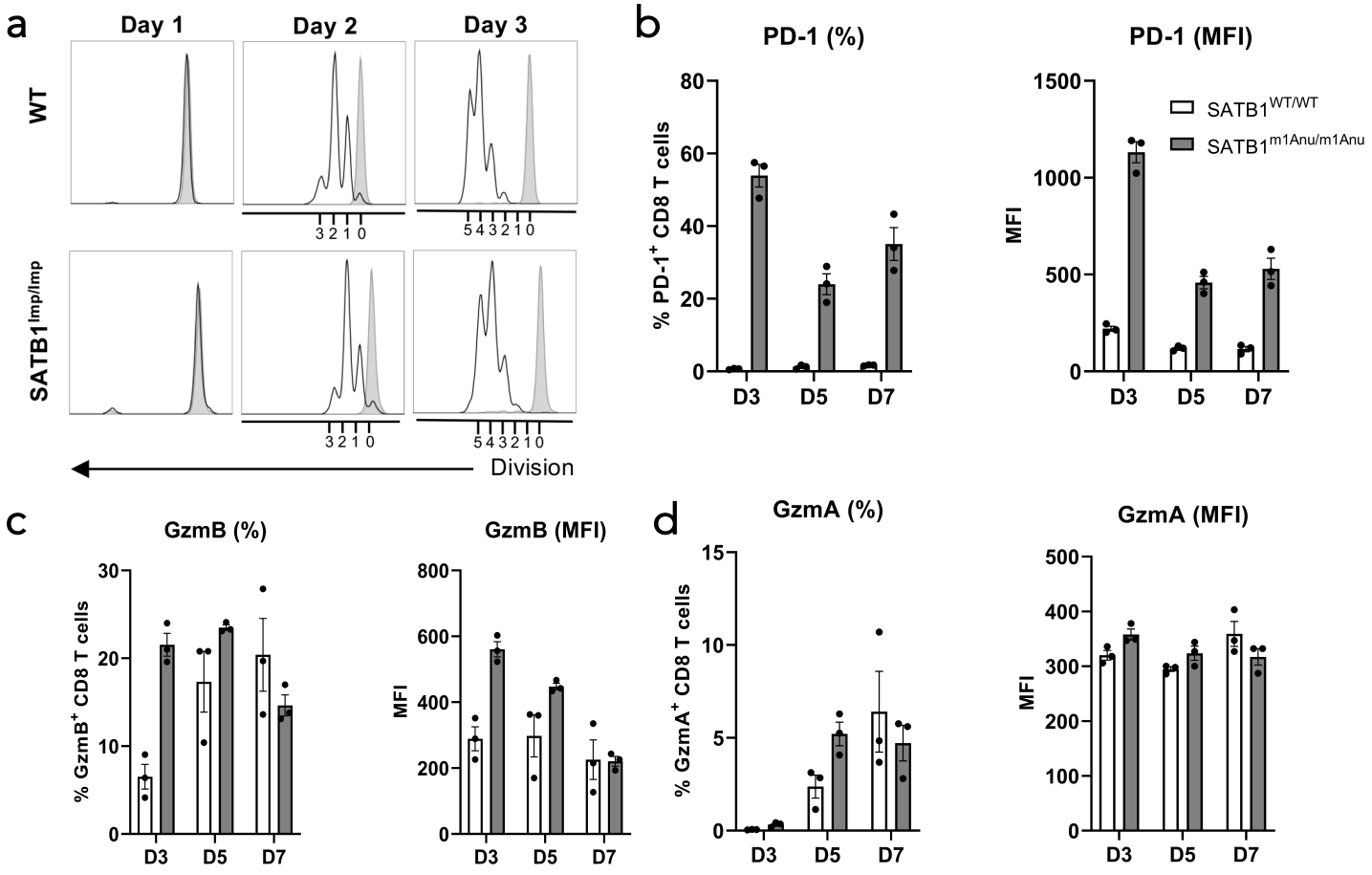

Supplementary figure 5. Increased effector marker expression after activation of SATB1$^{m1Anu/m1Anu}$ CD8^{+} T cells. **(a)** Naïve (CD44^{lo}CD62L^{hi}) CD8^{+} T cells from WT or SATB1$^{m1Anu/m1Anu}$ mice were sort purified and stained with Cell Trace Violet. Cells were then stimulated *in vitro* with αCD3/αCD8 (unshaded histogram) and the extent of cell division examined on days 1, 2 and 3 after activation Unstimulated controls are shown as an overlay (shaded histogram). Activated WT (white bars) or SATB1$^{m1Anu/m1Anu}$ CD8^{+} T cells were stained for PD-1 **(b)**, GzmB **(c)** or Gzm **(d)** on days 3, 5 and 7 after activation and proportion and mean fluorescence intensity (MFI) determined. Show are biological replicates. Statistical analyses used 2-way ANOVA with Sidak's multiple comparisons test. *P*-values: * $P < 0.05$, n = 3 mice per group; representative of two independent experiments.

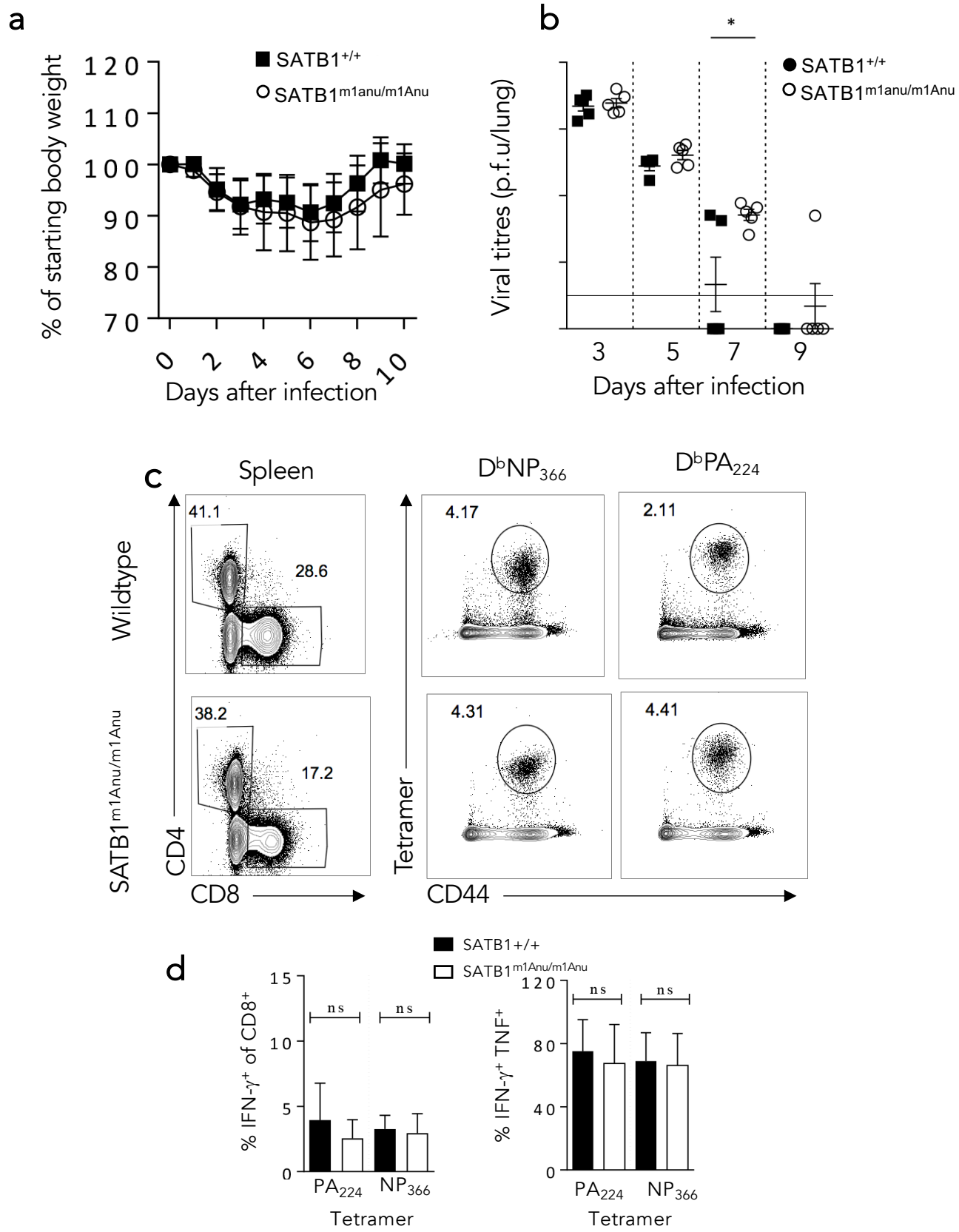

Supplementary figure 6. Delayed viral clearance in IAV infected SATB1$^{m1Anu/m1Anu}$ mice and induction of CD8^{+} T cell responses. **(a)** Both WT (SATB1$^{+/+}$) and SATB1$^{m1Anu/m1Anu}$ mice were infected intranasally with 10^3 p.f.u of A/HKx31 virus. Weight loss (% starting body weight) was measured at various times points after infection. **(b)** IAV viral titres were determined by plaque assay from perfused lungs from A/HKx31 infected WT and SATB1 SATB1$^{m1Anu/m1Anu}$ mice. **(c)** Splenocytes were isolated from WT or SATB1$^{m1Anu/m1Anu}$ mice 10 days after infection and stained with CD8 and either D^{b}NP$_{366}$ or D^{b}PA$_{224}$ tetramers. Shown are representative FACS plots. **(d)** Cytokine production of D^{b}PA$_{224}$ and D^{b}NP$_{366}$-specific CD8^{+} T cell isolated from the infected lung were assessed by intracellular cytokine staining 5 hours after *in vitro* stimulation with 1 µg of PA$_{224}$ or NP$_{366}$ peptide 10 days after infection.

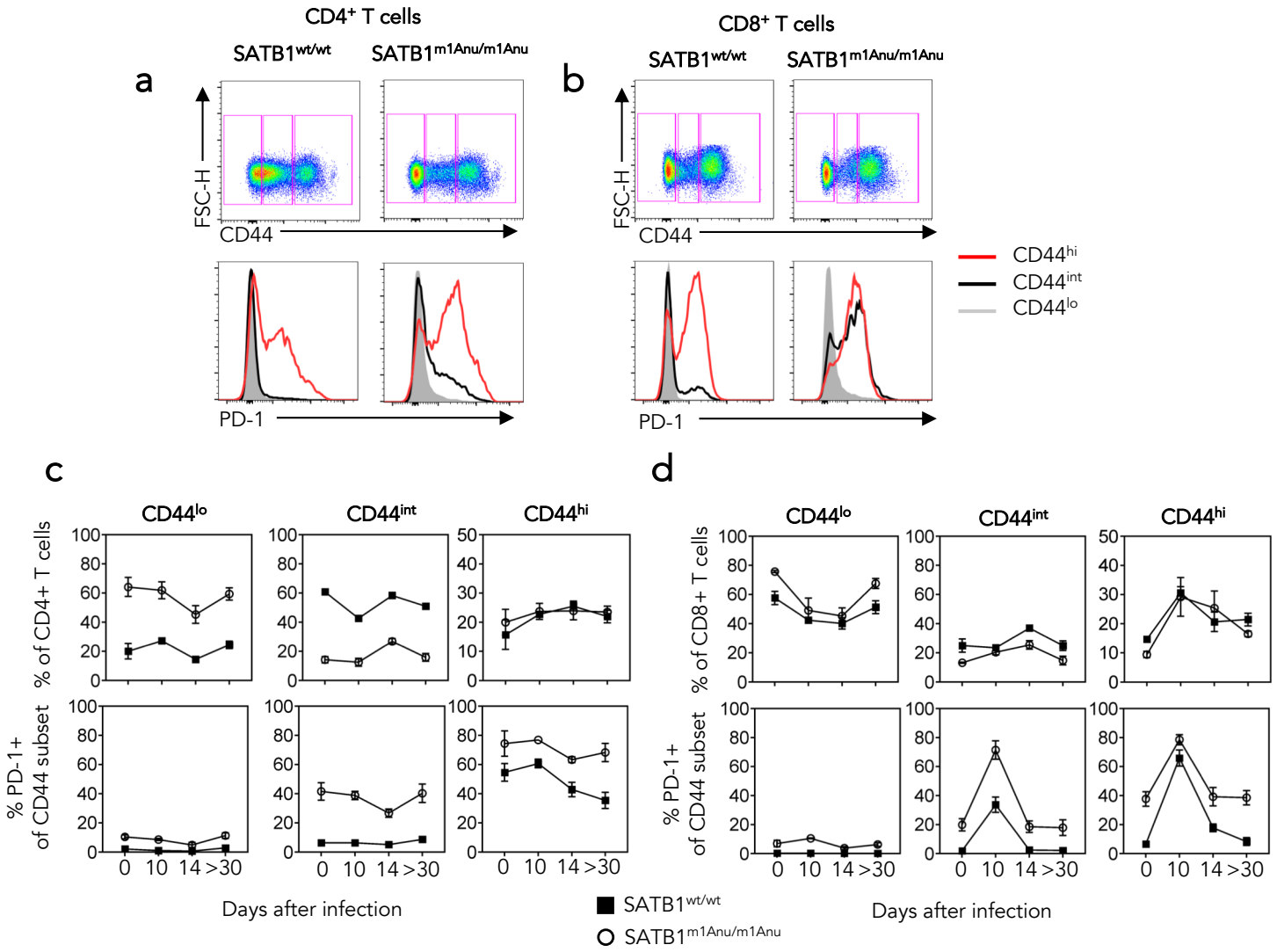

Supplementary figure 7. Higher baseline expression levels of PD-1 in SATB1$^{m1Anu/m1Anu}$ T cells. **(a, b)** Representative flow cytometry plots and histograms showing CD44 expression on CD4$^+$ **(a)** and CD8$^+$ **(b)** T cell populations from uninfected WT or SATB1$^{m1Anu/m1Anu}$ populations and subsequent PD-1 expression on CD44 subsets (histograms). **(c, d)** The proportion of CD4$^+$ **(c)**, or CD8$^+$ **(d)** T cells within each CD44 subset (top row) and the PD-1 expression within CD44 subsets (bottom row) isolated from uninfected mice, or at the indicated times after IAV infection (*x*-axis). Error bars show mean +/- SD of n = 2–5 mice per group, timepoint and surface staining from 2 or 3 independent experiments.

a

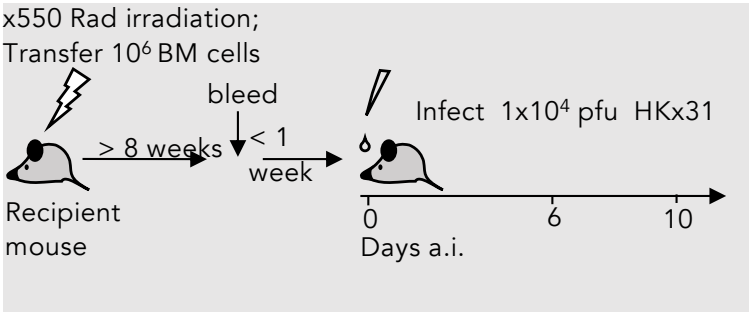

b

	Recipient (congenic marker)	Donor 1 (congenic marker)	Donor 2 (congenic marker)	x-axis labeling
1)	WT (CD45.1)	WT (CD45.2)	-	*$WT_{45.2}$*
2)	WT (CD45.1)	$SATB1^{m1Anu/m1Anu}$ (CD45.2)	-	*$SATB1^{m1Anu/m1Anu}$*
3)	$SATB1^{m1Anu/m1Anu}$ (CD45.2)	WT (CD45.1)	-	*$WT_{45.1}$*
4)	WT (CD45.1)	WT (CD45.1/2)	$SATB1^{m1Anu/m1Anu}$ (CD45.2)	*Mixed chimera: WT_{mix} and $SATB1^{m1Anu/m1Anu}$*

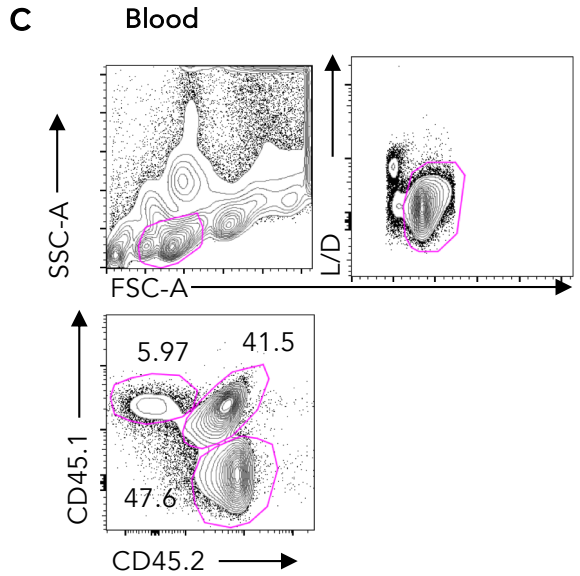

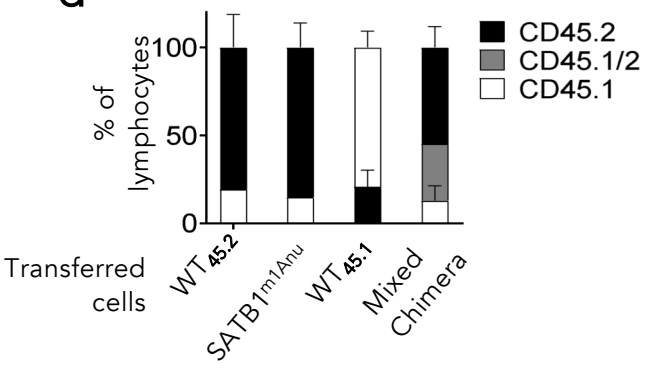

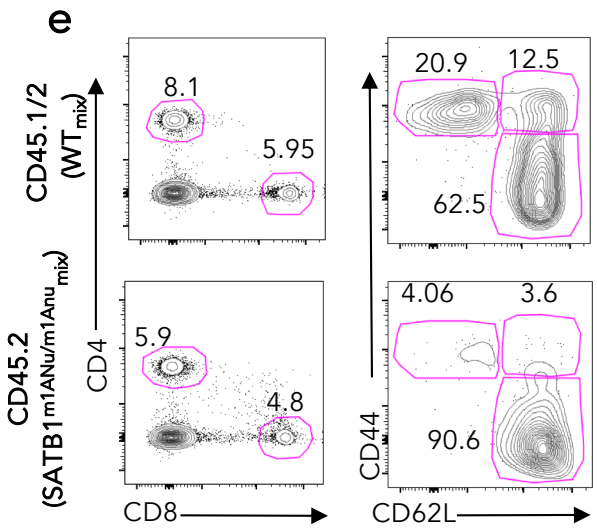

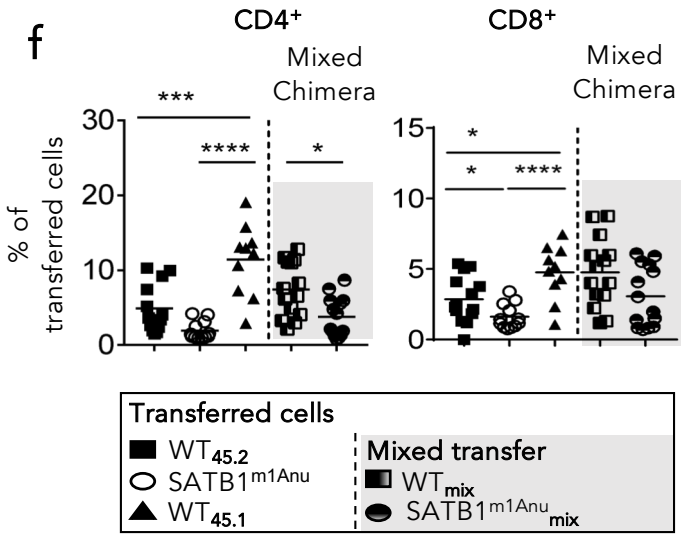

Supplementary figure 8. Generation of $SATB1^{m1Anu/m1Anu}$ and WT reconstituted bone marrow chimeras. (**a**) Scheme of irradiation, bleeding and infection of different bone marrow chimera groups. (**b**) Table showing the different bone marrow cell transfers into recipient mice for respective generated bone marrow chimera groups. (**c-d**) Representative FACS plots and quantitation of the proportions of donor bone marrow from blood of mixed chimeras. (**e-f**) Representative FACS plots and the percentage of $CD4^+$ and $CD8^+$ T cells in blood of different bone marrow chimera groups > 8 weeks after irradiation and bone marrow transfer. 5 - 8 mice per bm group, representative of 3 independent experiments. Unpaired Students *t*-test analysis *(P*-value * $P \leq 0.05$; ** $P \leq 0.01$, *** $P \leq 0.001$, **** $P \leq 0.0001$).